

Supporting Information

**Tracing Experimentally Compatible Dynamical and Structural Behavior of
Atmospheric N₂/O₂ Binary Mixtures within Nanoporous Li-LSX Zeolite:
New Insights to Influence of Extra-Framework Cations by MD Simulations**

Mohammad H. Kowsari*

*Department of Chemistry and Center for Research in Climate Change and Global Warming (CRCC),
Institute for Advanced Studies in Basic Sciences (IASBS), Zanjan 45137-66731, Iran*

* Corresponding author. Tel.: +98 24 3315 3207. Fax: +98 24 3315 3232.
E-mail address: mhkowsari@iasbs.ac.ir , mohammad.kowsari@gmail.com (M. H. Kowsari).

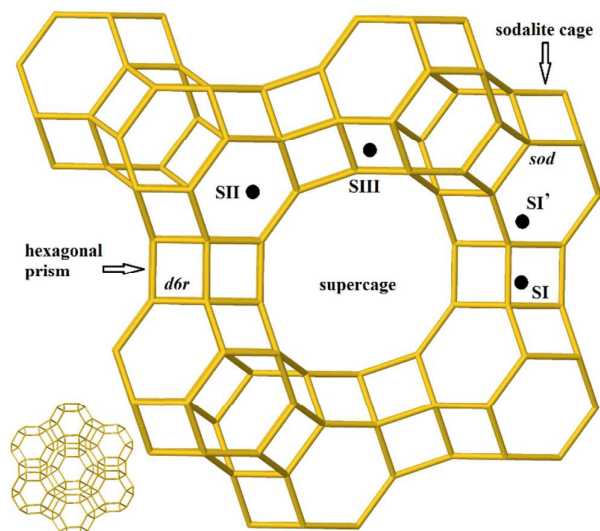


Figure S1. The main types of cation positions (SI, SII, and SIII) in the framework of faujasite based of Lobo crystallography data for Li-LSX zeolite [Feuerstein, M.; Lobo, R. F.; *Chem. Mater.* **1998**, *10*, 2197-2204].

The framework is drawn by online Jsmol (a JavaScript-based viewer for three-dimensional chemical structures) linked in the website of the database of zeolite structures:

<http://www.iza-structure.org/databases/>.

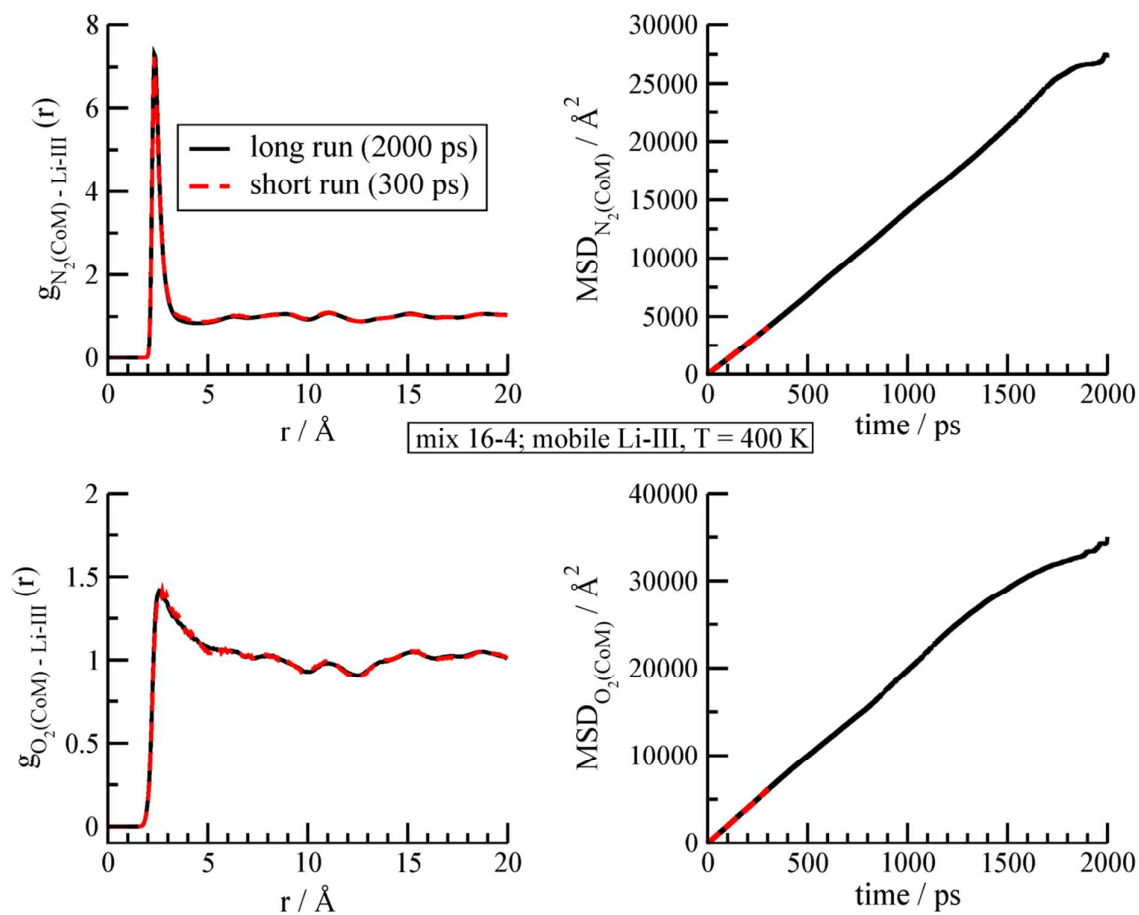


Figure S2. Investigation of the effect of simulation run-time on the (guest--Li-III) RDFs and the center of mass MSDs of guest molecules from binary air mixture simulations of (16 N_2 + 4 O_2) per unit cell of Li-LSX zeolite with mobile Li-III at 400 K.

In general, the run-time ~ 1000 -2000 ps is recommended for obtaining a good linear diffusive regime of MSD plots of guest species at low temperatures.

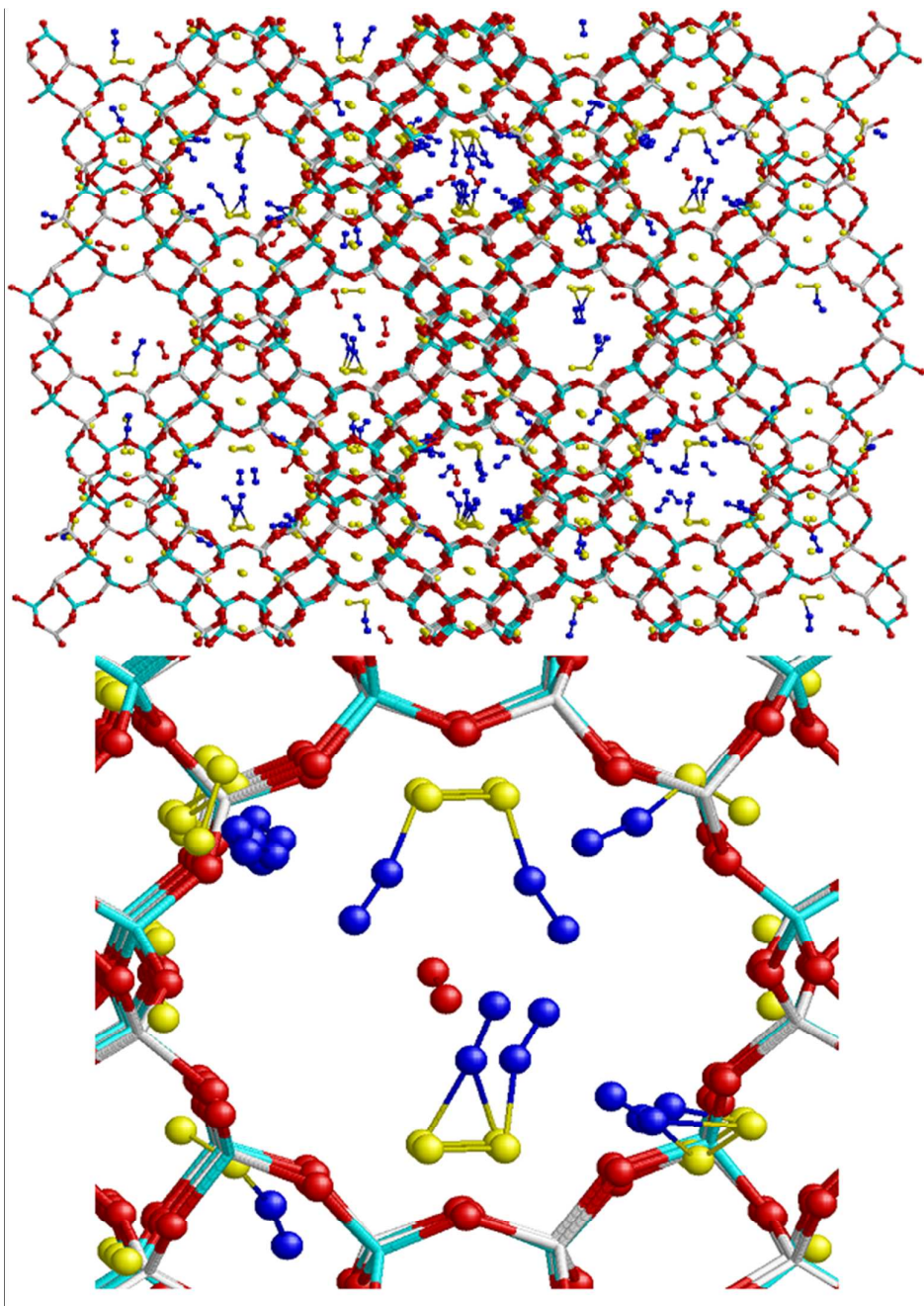


Figure S3. Sample snapshot of the simulation box of “mix 16-4” at 298 K within the framework of Li-LSX zeolite with fixed Li-III sites (yellow colour) viewed along [110]. It includes the distribution of N₂ (blue colour) and O₂ (red colour) guest at 298 K and a close-up view of a supercage of the Li-LSX zeolite. The (N--Li-III) distances are in the range of 1.67-1.81 Å. The red, white, and cyan colours represent O, Al, and Si sites of zeolite, respectively.

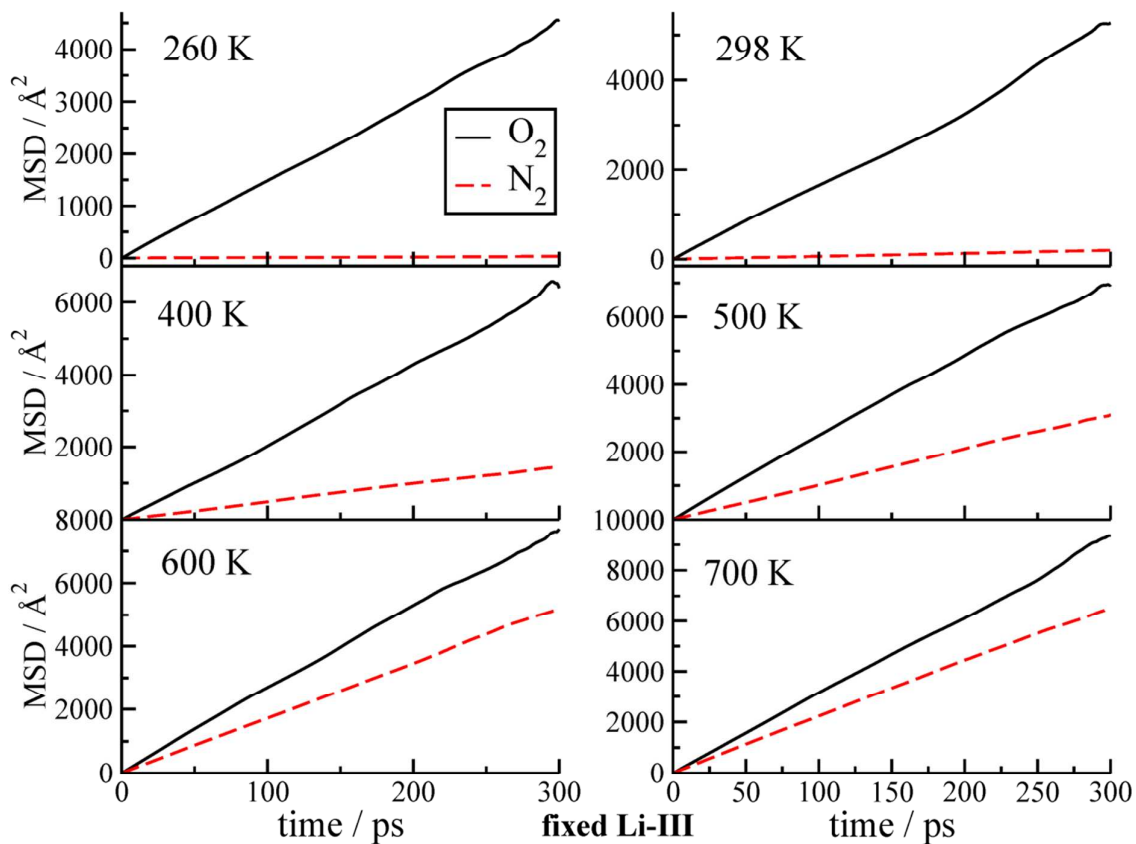


Figure S4. Comparison of the computed center of mass MSD of N_2 and O_2 within nanopores of Li-LSX zeolite from “mix 16-4” simulations with fixed Li-III cationic sites at different temperatures. O_2 diffuses inside the zeolite faster than N_2 .

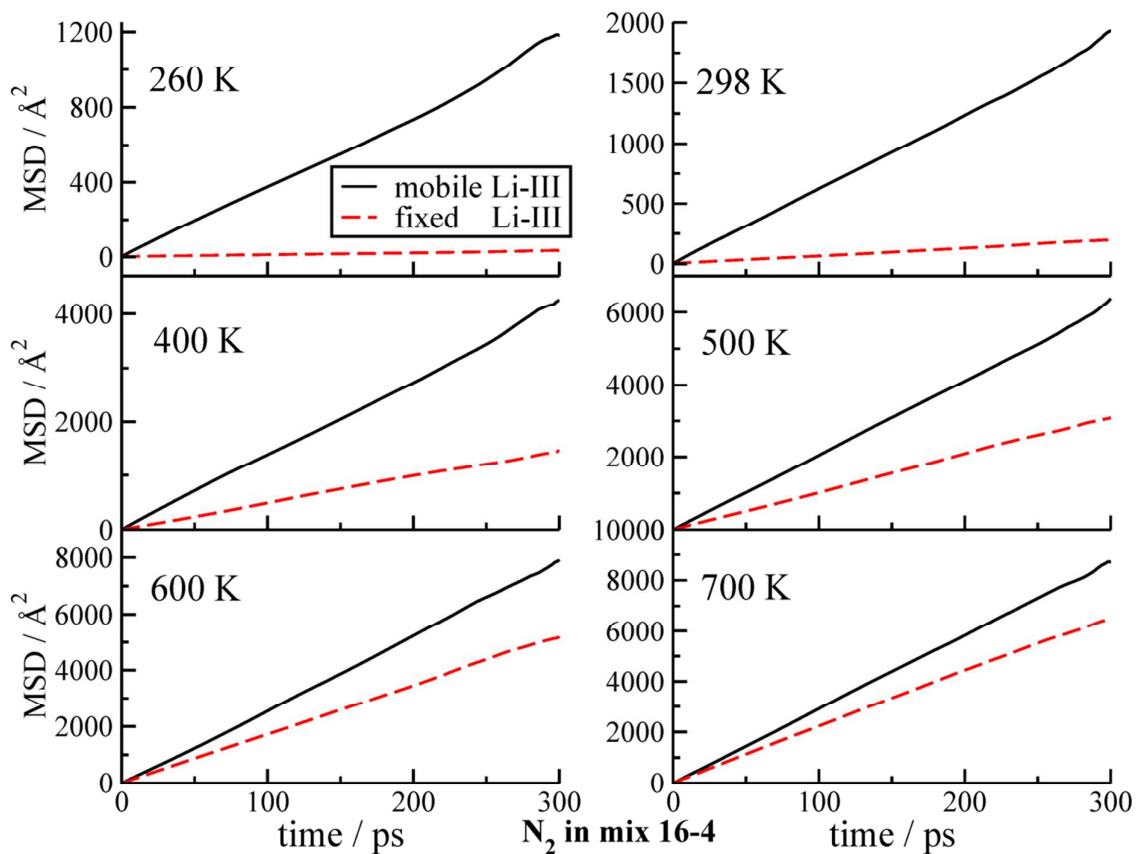


Figure S5. Effect of simulations with fixed or mobile Li-III cationic site on the computed center of mass MSD of N_2 within nanopores of Li-LSX zeolite for “mix 16-4” simulations at different temperatures. The MSD of N_2 is sensitive to the fixed/mobile Li-III situation.

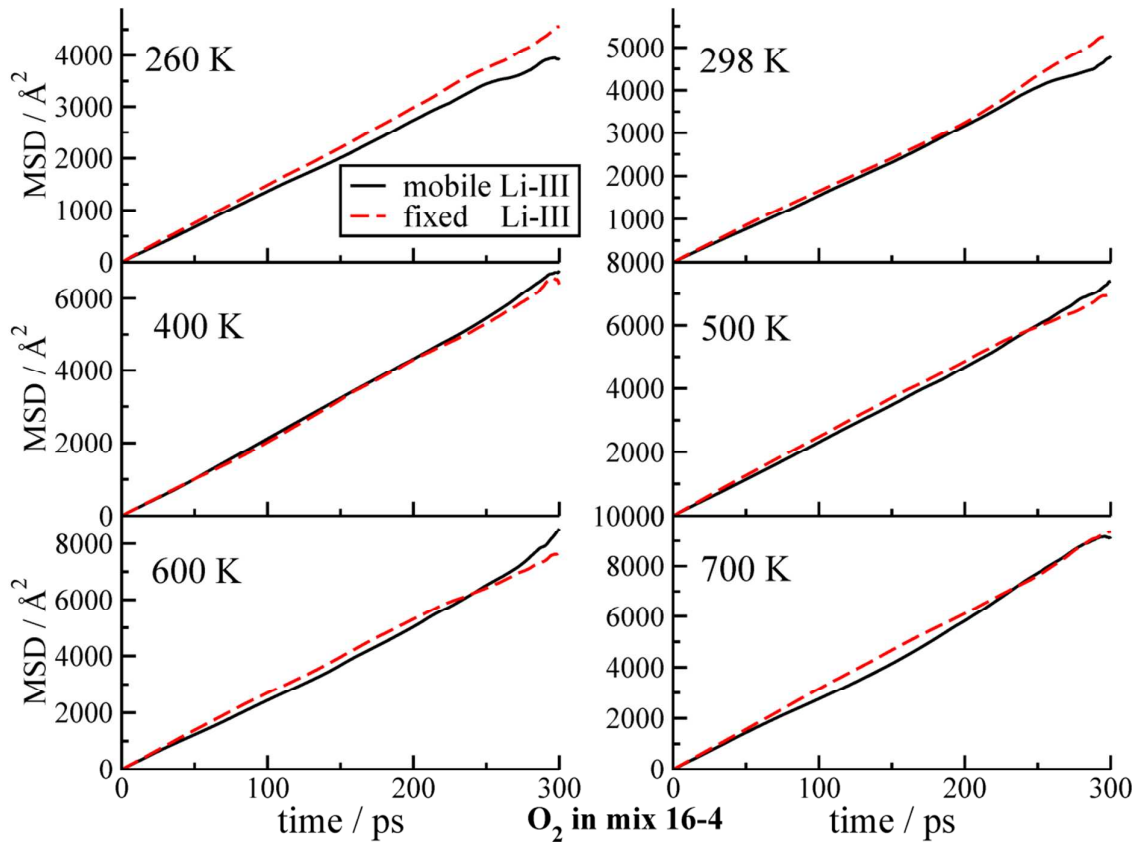


Figure S6. Effect of simulations with fixed or mobile Li-III cationic site on the computed center of mass MSD of O₂ within nanopores of Li-LSX zeolite for “mix 16-4” simulations at different temperatures. The MSD of O₂ is not sensitive to the fixed/mobile Li-III situation.

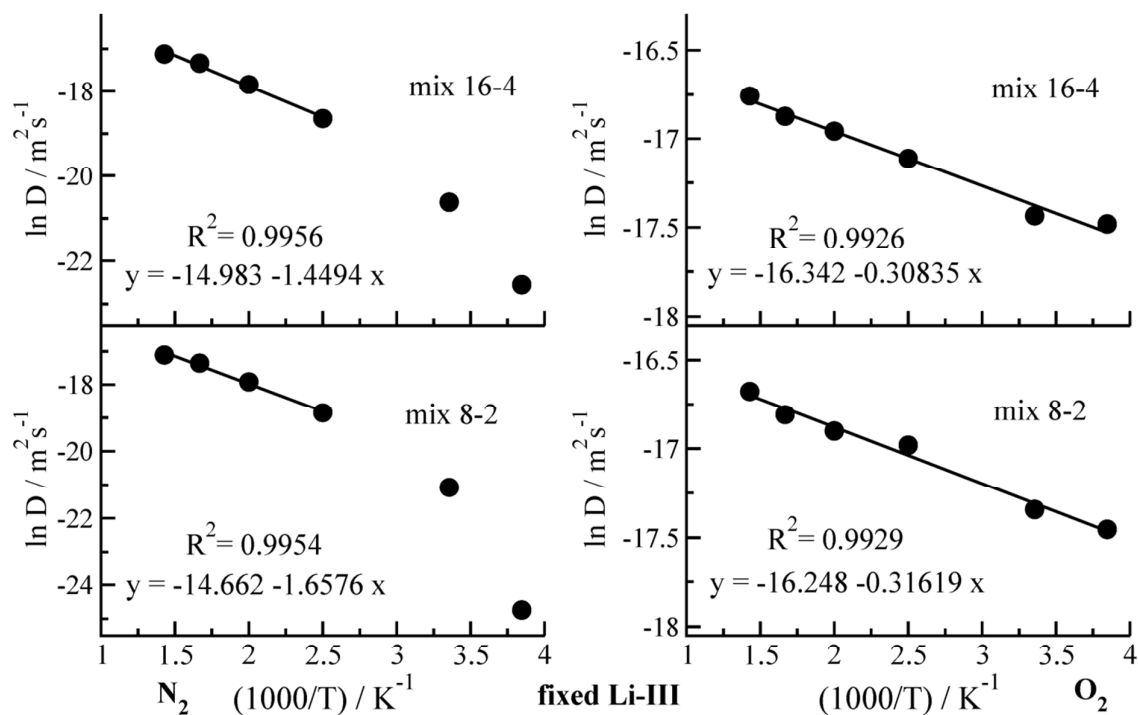


Figure S7. Arrhenius plots of the natural logarithm of the self-diffusion coefficient of N_2 and O_2 versus the inverse temperature $1/T$, for determining activation energy of diffusion within Li-LSX zeolite for two studied binary mixtures with fixed Li-III situation.

The left panels of Figure S7 include the simulated data for N_2 at 298 and 260 K from simulations with fixed Li-III, but these are not included in the fit of the Arrhenius plot since they deviate from the straight line of the higher temperature points. The left panels show that a new solid-like diffusion regime may be operating for N_2 at low temperatures. Indeed, it seems that the slowing of the motion of N_2 molecules in the MD simulations with fixed Li-III at the lower studied temperatures (298 and 260 K) proceeds much stronger than expected by the Arrhenius law for thermally activated motions. This causes the lower computed diffusion coefficient for N_2 in Li-LSX zeolite at 298 and 260 K, when the fixed Li-III situation used in simulations, compared with the expected value based on the Arrhenius law.

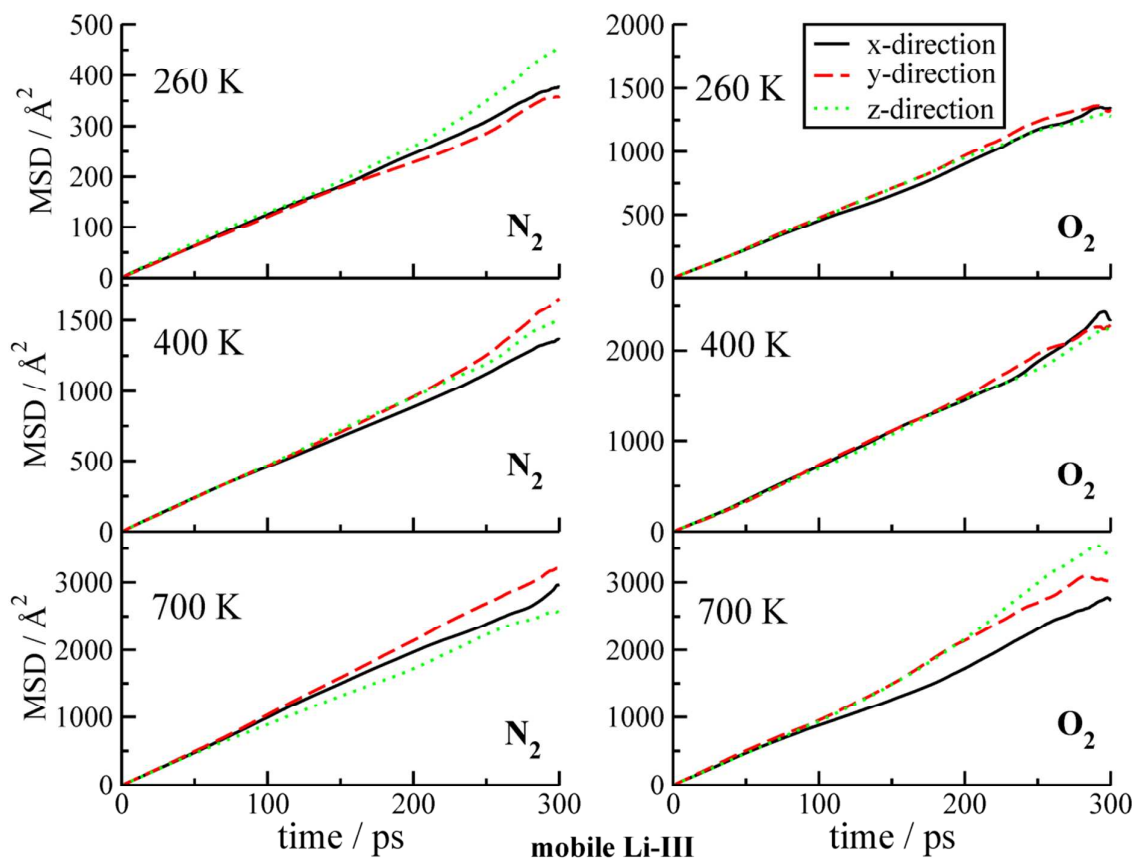


Figure S8. Computed explicit center of mass MSD components of N_2 and O_2 in the x-, y-, and z-directions within nanopores of Li-LSX zeolite for “mix 16-4” simulations with mobile Li-III at 260, 400, and 700 K. The MSD preference cannot be seen in a certain direction.

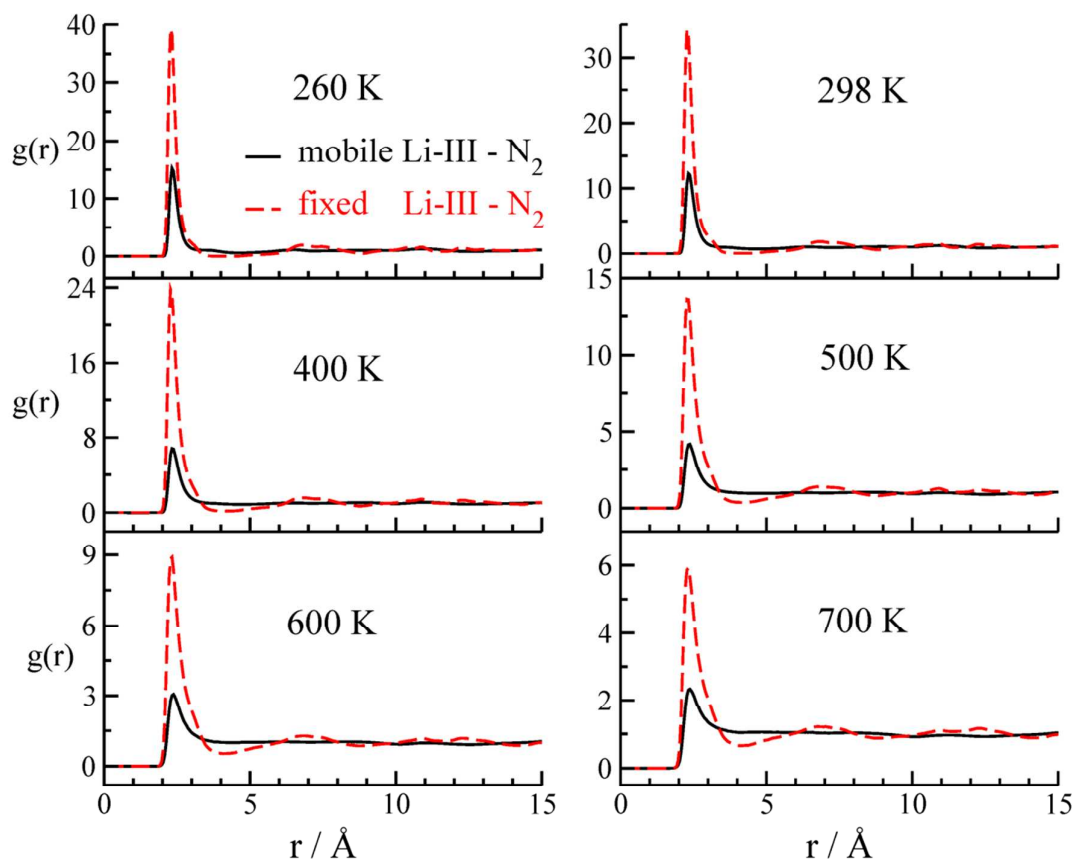


Figure S9. Effect of simulations with fixed or mobile Li-III cationic site on the computed (Li-III - N₂) RDF for “mix 16-4” simulations at different temperatures. The structural correlation between N₂ molecules and fixed Li-III sites is higher than that of for mobile Li-III sites. The RDFs from the simulations at the fixed Li-III condition also show several short oscillating peaks at sights near the fixed location of the Li-III sites in these simulation runs.

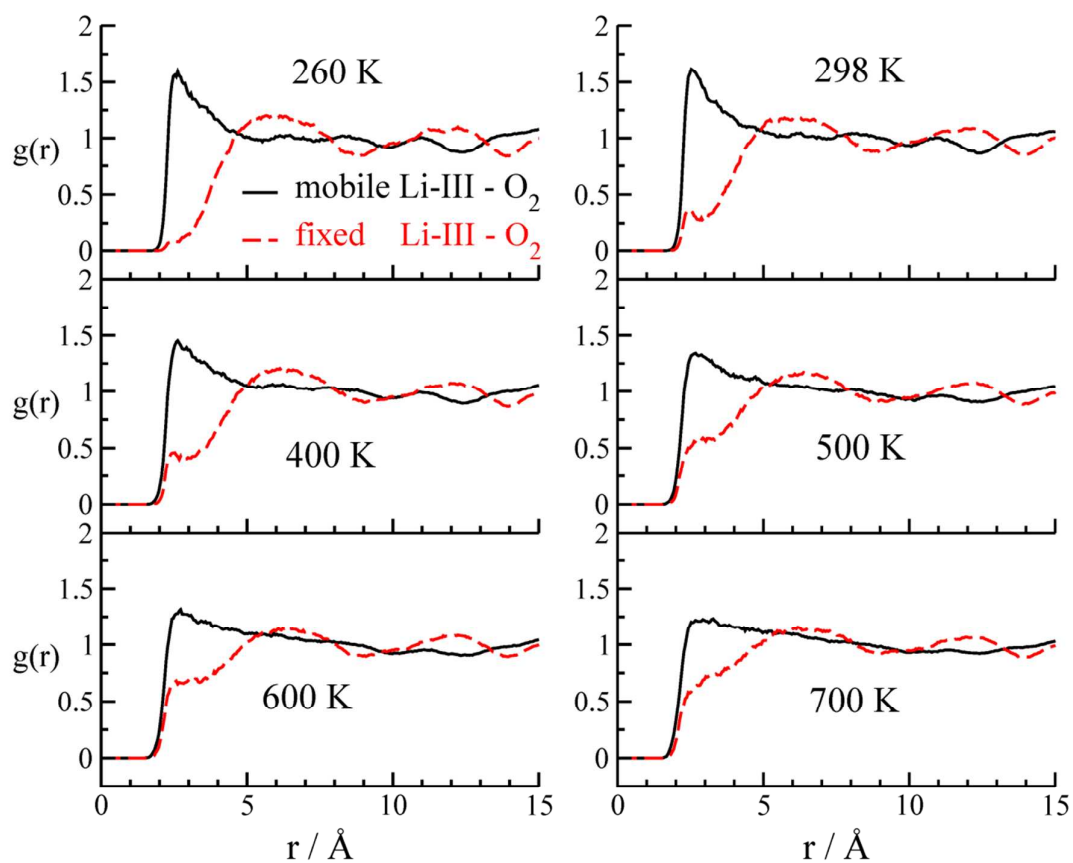


Figure S10. Effect of simulations with fixed or mobile Li-III cationic site on the (Li-III - O₂) RDF for “mix 16-4” simulations at different temperatures. There is no measurable structural correlation between O₂ molecules and Li-III cations. Several short oscillating peaks at sights near the fixed Li-III location can be observed.

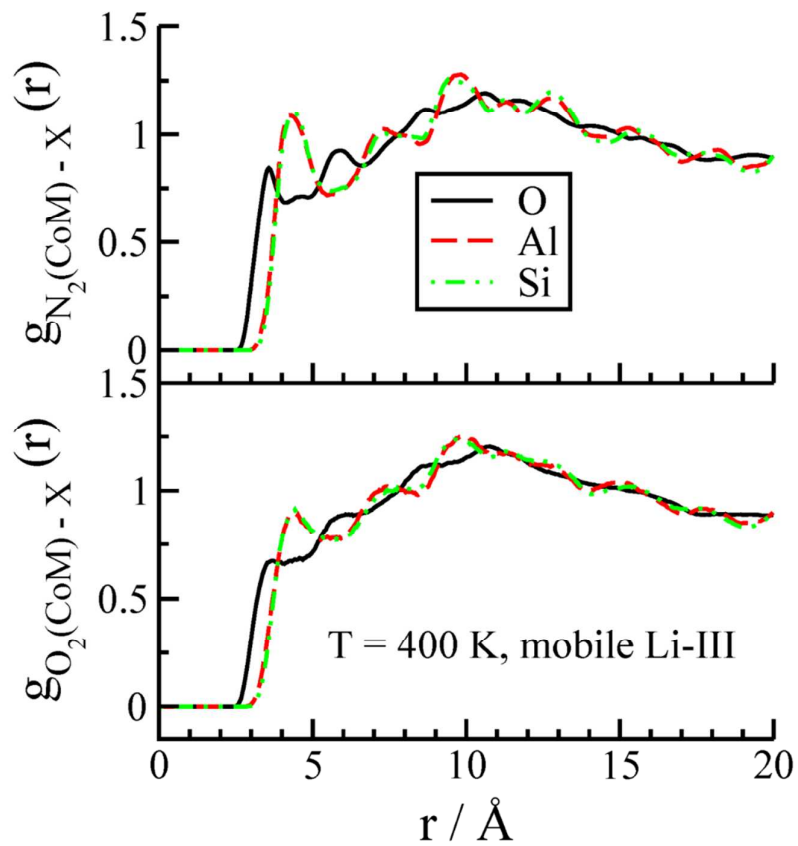


Figure S11. The RDF between the center of mass of N_2 or O_2 and O, Al, and Si atoms of Li-LSX zeolite framework from “mix 16-4” simulation with mobile Li-III cations at 400 K.

The applied basic relations for computing the different quantities

The dynamical behavior and the microscopic motion of the N₂ and O₂ is studied by calculating the MSD and reduced VACF of these species from MD simulations of studied binary mixtures in Li-LSX zeolite using the following relations,

$$\text{MSD}(t) = \frac{1}{N} \sum_{i=1}^N \langle [\mathbf{r}_i^c(t) - \mathbf{r}_i^c(0)]^2 \rangle \quad (1)$$

$$\text{VACF}(t) = \frac{1}{N} \sum_{i=1}^N \frac{\langle \mathbf{v}_i^c(t) \cdot \mathbf{v}_i^c(0) \rangle}{\langle \mathbf{v}_i^c(0) \cdot \mathbf{v}_i^c(0) \rangle} \quad (2)$$

where $\mathbf{r}_i^c(t)$ and $\mathbf{v}_i^c(t)$ are the position and the velocity of the center of mass of the particle i at time t and the brackets $\langle \rangle$ represent an ensemble average over all time origins. Both MSD and VACF are the single-particle correlation functions and their statistical precision is improved by averaging over all particles in the system.

From the molecular point of view, the self-diffusion coefficient gives a microscopic detailed description of the single particle motion. We calculate the self-diffusion coefficient of each guest component from the slope of long time limit of the MSD using well-known Einstein relation,

$$D_i = \frac{1}{6N} \lim_{t \rightarrow \infty} \frac{d}{dt} \sum_{i=1}^N \langle [\mathbf{r}_i^c(t) - \mathbf{r}_i^c(0)]^2 \rangle \quad (3)$$

To determine whether the diffusion is in the linear regime, the slope of the log-log MSD plot is used to calculate the quantity β factor defined by,

$$\beta(t) = \frac{d \log(\text{MSD}(t))}{d \log(t)} \quad (4)$$

If β is very close to 1, the good linear regime for calculation of self-diffusion is determined.

To calculate the diffusion activation energy, Arrhenius equation is used,

$$D = D_0 e^{\frac{-E_{\text{act}}}{RT}} \quad (5)$$

where E_{act} , R , and T are activation energy, gas constant, and temperature, respectively.

The diffusion selectivity, S_{diff} , can be taken from the MD simulation of a binary guest mixture by computing the ratio of the self-diffusivities of species in the mixture:

$$S_{\text{diff}} = \frac{D_{1,\text{self}}}{D_{2,\text{self}}} \quad (6)$$

The radial distribution function (RDF) shown by $g(r)$, determines the local structural of atoms relative to each other and can be obtained from MD simulations. For a system of N atoms in a volume V (with number density ρ), the RDF is defined by the expression:

$$\rho g(r) = \frac{1}{N} \langle \sum_{i=1}^N \sum_{j \neq i}^N \delta(r - r_{ij}) \rangle \quad (7)$$

where the bracket indicates time average and r_{ij} is the distance between atoms i and j .